https://doi.org/10.1016/j.engstruct.2020.110651

Rocking bridge piers equipped with shape memory alloy (SMA) washer springs

Cheng Fang [1,2], Dong Liang [1], Yue Zheng [1*], Michael CH Yam [3], Ruiqin Sun [1]

[1] *College of Civil Engineering, Tongji University, Shanghai 200092, China*
[2] *Shock and Vibration of Engineering Materials and Structures Key Laboratory of Sichuan Province, Mianyang 621999, China*
[3] *Department of Building & Real Estate, The Hong Kong Polytechnic University, Hung Hom, Kowloon, Hong Kong, China*
** Corresponding author: email: yzheng@tongji.edu.cn, Tel: +86 (0)21-65982926*

Abstract: The emergence of rocking bridge piers provides the community of civil engineers with a broader vision of next-generation seismic-resilient bridge design. This study introduces a new type of shape memory alloy (SMA) washer spring-based self-centering rocking (SCR) systems which could be an important addition to the existing rocking pier family. The proposed system combines the advantage of the existing rocking pier solution with extra benefits such as simplified construction, excellent fatigue and corrosion resistance, and extra "locking mechanism" which safely prevents the pier from excessive rocking. The working principle of the SCR piers is discussed first, and five tests are subsequently carried out on proof-of-concept SCR pier specimens. This is followed by a further numerical study examining an extended range of design parameters. The SCR pier shows excellent self-centering capability with minimal damage to the pier, which is attributed to the intended gap-opening deformation mode. Moderate energy dissipation is offered by the SMA washer springs, and once they are fully flattened, further drift is provided by the flexural deformation of the pier itself. The SMA washers can be used repeatedly with no need for repair/replacement, and the highly flexible stack pattern caters to different design objectives and requirements. An effective supplementary source of energy dissipation is enabled by installing steel angles at the gap opening interface. The experimental and numerical investigations provide a strong proof of feasibility of this innovative structural system.

Keywords: Rocking bridge pier; shape memory alloy (SMA); self-centering; Belleville washer springs; cyclic performance; seismic resilience.

1. Introduction

Major earthquakes in recent decades highlighted the importance of considering post-event recoverability in the design of lifeline facilities such as strategic buildings, power facilities, piping systems, and bridges. Field investigations made after the 1995 Kobe earthquake reported that more than 90 reinforced concrete (RC) bridge piers with residual drifts exceeding 1% were demolished, although they did not collapse [1]. The repair/replacement work leads to closure of the bridges and hinders the initiation of recovery, resulting in significant economic and societal impacts on the city. There is a pressing need for a fundamental shift in the design targets for bridges and other critical infrastructures in seismic zones. To this end, many new technologies have been developed for resilient engineering systems that are capable of surviving strong earthquakes with negligible residual deformation and no critical damage to the main part of the structure [2-3].

Self-centering rocking (SCR) bridge piers are one of these promising solutions. In contrast to conventional fixed base monolithic bridge piers where plastic deformation is expected to occur locally at the base regions, the SCR piers allow gap opening over the rocking interface, a mechanism which significantly alleviates the local plasticity demand at the pier base. Vertical unbonded posttensioned (PT) tendons are often used in SCR piers to promote reversion to the upright position (i.e., self-centering capability), and in addition, various types of energy dissipation devices, either internal or external, are employed concurrently to avoid excessive drifts. Mander and Cheng [4] launched an experimental program on low-damage rocking bridge piers, and this work inspired many follow-up investigations. Palermo et al. [5] confirmed the unique behavior of SCR piers in regard to ductility and residual drift control through comparisons against traditional monolithic piers. Solberg et al. [6] carried out a series of cyclic tests focusing on the behavior of SCR piers under bidirectional earthquake excitations. Marriott et al. [7-8] conducted a series of quasi-static and pseudo-dynamic tests on SCR piers with replaceable energy dissipation devices. Guerrini et al. [9] proposed a new type of PT double-skin concrete-filled SCR piers. The design criteria for the pier members was discussed in detail, and tests on two pier units showed no damage at a target drift of 3%. Rahmzadeh et al. [10] proposed a new SCR pier system consisting of a tubular steel column, PT tendons, and

energy dissipation devices, with focus on the stress concentration and local buckling behavior of the tube wall near the rocking interface. It should be noted that the conventional rocking piers may not have sufficient redundancy if the prestress of the PT tendons is lost under extreme load conditions. This could lead to excessive rocking and also the risk of collision between the girder and the abutments [11]. In addition, the energy dissipation devices often need to be replaced after strong earthquakes, and this process puts the bridge in danger during aftershocks [12]. The corrosion of the PT tendons and energy dissipation devices is also a big problem [13]. Guo et al. [14] examined a variety of fiber-reinforced polymer PT tendons and energy dissipaters to cater to the chloride environment, and it was confirmed that the composite materials can provide satisfactory self-centering and energy dissipation capacities.

The concept of SCR is also widely applied to precast segmental construction, in which case more than one gap opening interfaces may be developed over the column height [15]. Prefabricated segmental bridge piers can speed up the construction process, and are therefore quite popular in congested urban regions [16-17]. A large number of experimental investigations have been conducted on this front [18-22], with many follow-up numerical and analytical studies carried out to further interpret the load carrying mechanism of the system [23-24]. Furthermore, the use of the self-centering technology has been extended to high-performance building frames, where self-centering beam-to-column connections and rocking columns/walls have attracted significant attention for residual drift control [25-36].

This paper presents an alternative type of SCR bridge piers which employ novel superelastic shape memory alloy (SMA) washer springs as the kernel functional components. SMAs are a unique class of metal exhibiting two fundamental properties, namely, superelasticity (SE) and shape-memory effect (SME) [37-41]. The former occurs when the material is stressed at its austenite phase, where a 8-10% strain can be recovered spontaneously upon unloading; the latter is exhibited by the martensite form of the SMA, in which case residual strain does remain when the applied stress is removed (just like normal steel), but heating the deformed material to the austenite-finish temperature can promote

strain recovery. Due to the two special characteristics, SMAs have been successfully commercialized in the aerospace, medical, electrical, and oil industries [42]. Compared with the shape-memory effect, superelasticity seems to receive more attention for seismic applications due to spontaneous self-centering, stable hysteretic damping, and free of external power source/electricity supply. In practice, superelastic SMAs are often made into various forms such as SMA wires, cables, bars, ring springs, helical springs, and washer springs [43-48]. When used in SCR piers, the SMA components can provide self-centering capability and energy dissipation due to the flag-shaped stress-strain relationship of the material.

In the following discussions, the basic working principle of the proposed SCR piers is first introduced, and their potential advantages over the current PT tendon-based SCR pier solutions are discussed. Five proof-of-concept tests on the novel SCR pier are then described, which is followed by a numerical study considering an extended range of design parameters. Some design comments are also given.

2. System description

SMA washer springs (also known as disc springs) are the kernel components that provide self-centering capability and energy dissipation for the newly proposed SCR pier system. Conventional steel washer springs are mechanical components that are capable of sustaining loads with a small installation space, as shown in Fig. 1(a). Because of their annular shape, force transmission is concentric and thus the washer springs can be more stable and compact compared with other types of springs, e.g. helical springs. Importantly, washer springs can be stacked either in parallel or in series (or in combination), which makes them flexible in terms of load resistance and available deformability. The application of the washer springs can be further extended when they are endowed with superelasticity [49]. In fact, a number of investigations have already been initiated to explore the potential applications of SMA washer springs in civil engineering, including smart dampers [50] and high-performance beam-to-column connections [51].

The new SCR pier system consists of a concrete pier (with an extended base), a series of strong constraining anchor bars, and the associated SMA washer spring sets, as shown in Fig. 2. The vertical constraining anchor bars are inserted permanently into the foundation, while the free parts pass through the openings of the pier base. The SMA washer spring sets, which pass through these anchor bars, are installed and simply precompressed by tightening the nuts. If a further increase in the resistance of the piers against lateral load is desired, unbonded PT tendons running through the height of the pier may be additionally used. However, unlike the existing PT-based SCR piers, the use of the PT tendons is not compulsory for the present SCR piers as the preloaded SMA washer springs can provide sufficient load resistance and self-centering capability.

As shown in Fig. 2, the pier deforms elastically and exhibit a load-deflection response similar to a fixed base pier before "decompression" of the preloaded SMA washer springs. As the lateral load increases, the pier starts to uplift with a gap opening mechanism at the rocking interface. During this inelastic stage, the SMA washer springs are further compressed until their deformability has been fully consumed and then a "locking" mechanism is formed (Fig. 2(d)). This locking mechanism safely constraints the pier and prevents it from excessive rocking. A further increase in the lateral load would stress the anchor bars, and later on inelastic deformation could occur in the main pier. Under extreme cases (e.g., very rare earthquakes), the anchor bars may also undergo inelastic deformation and finally fail in fracture or pulling-out from the foundation. This unfavorable failure mode should be prevented by making sure that the final failure is always governed by the pier rather than by the anchor bars. The SMA washer springs together with the gravity load promote self-centering action which helps the pier return to its original upright position, ideally with no damages to the main pier, anchor bars and SMA washer springs under design earthquakes. The SMA washer springs also act as a source of energy dissipation due to their superelastic behavior.

Fig. 3 shows more detailed force decomposition diagrams of the pier and takes a closer look at the force distribution over the rocking interface. Under an increasing lateral load (and hence an increasing overturning moment), the pier experiences "decompression stage" (where the gap is just

about to open), "post-decompression stage", and "locked stage" successively. Assuming that the edge of the extended pier base, i.e., point *c*, serves as the reference turning point, the overturning moment of the pier *M* at the decompression stage (Fig. 3(a)) can be expressed by:

$$M = \sum F_{w1-pre} l_{w1} + \sum F_{w2-pre} l_{w2} - F_{cc-De} l_{cc} + F_G l_{mid} \tag{1}$$

$$F_{cc-De} = \sum F_{w1-pre} + \sum F_{w2-pre} + F_G = 0.5 \varepsilon_{max} E_c A_c \tag{2}$$

where F_G is the axial load applied to the pier; $F_{w\text{-}pre}$ is the preload of the SMA washers; $F_{cc\text{-}De}$ is the resultant reaction force from the foundation; l_{w1}, l_{mid}, l_{w2} and l_{cc} are the lever arms, i.e., the distances from the force (or resultant force) to the assumed turning point; ε_{max} is the maximum compression strain of concrete at the edge of the pier base; E_c is the elastic modulus of concrete; A_c is area of the pier base; and Σ indicates the sum of the washer spring forces if more than one set of washers are used at the considered locations.

In the post-decompression stage, an idealized linear strain distribution may still be assumed for the contact region [52], as shown in Fig. 3(b). The equilibrium of forces can be expressed by [53]:

$$M = \sum (F_{w1-pre} + \Delta F_{w1}) l_{w1} + \sum \left(F_{w2-pre} + \Delta F_{w2}\right) l_{w2} - F_{cc-P} l_{cc} + F_G l_{mid} \tag{3}$$

$$F_{cc-P} = \sum (F_{w1-pre} + \Delta F_{w1}) + \sum (F_{w2-pre} + \Delta F_{w2}) + F_G = 0.5 \varepsilon_{max} E_c l_c b_c \tag{4}$$

where ΔF_{w1} and ΔF_{w2} are the increments of the force of the SMA ring spring washers; l_c is the length of the triangular stress block; and b_c is the width of the pier base. Finally, at the locked stage, the opening of the pier base may cause local concrete crushing near the turning point, so the strain distribution of the concrete could be highly nonlinear. For simplicity, the nonlinear strain distribution can be simplified as a uniform block, as shown in Fig. 3(c), and the equilibrium of forces can be expressed by:

$$M = \sum (F_{w1-pre} + \Delta F_{w1}) l_{w1} + \sum (F_{w2-pre} + \Delta F_{w2}) l_{w2} - F_{cc-L} l_{cc} + F_G l_{mid} \tag{5}$$

$$F_{cc-L} = \sum (F_{w1-pre} + \Delta F_{w1}) + \sum (F_{w2-pre} + \Delta F_{w2}) + F_G = \varepsilon_p E_c l_{cp} b_c \tag{6}$$

where $F_{cc\text{-}L}$ is the resultant reaction force near the turning point, l_{cp} is the length of the idealized stress block; and ε_p is the uniform plastic strain of the concrete.

Compared with the existing PT-based SCR piers described in the literature, the SMA-based ones proposed in this study may have the following extra benefits: 1) PT tendons are not compulsory, which simplifies the construction process, reduces the preload applied to the pier, and eliminates the risk of loss of self-centering capability due to the possible yielding or stress relaxation of the PT tendons; 2) a flexible use of the SMA washer springs enables tunable deformation and lateral load resistance; in addition, the presence of the strong constraining anchor bars prevents excessive uplifting of the pier; 3) due to the stable hysteretic behavior and good fatigue performance of SMA washer springs under repeated load, there is no need to replace or repair these components after earthquakes, and thus ensuring immediate function recovery; and 4) in contrast to steel energy dissipators and tendons that have corrosion problems, the SMA material has excellent corrosion resistance, which encourages the SCR piers to be used in chloride environments.

In practice, the following design principles for the proposed pier are recommended: 1) no uplift occurs under small earthquakes with a return period of 50 years; in other words, the rocking pier is expected to behave just like a conventional fixed-base pier before decompression of the SMA washers; (2) limited uplifting with a well-controlled lateral drift ratio (e.g., 1.0%) of the rocking pier is permitted to protect the bridge from damage when subjected to moderate earthquake events with a return period of 475 years; and (3) the bridge is expected to experience a larger lateral drift ratio (e.g., 2.5%) but with controlled damage under large earthquake events with a return period of 2500 years. The SMA washers may be fully flattened under large earthquakes, in which case the bridge would rely on the locking mechanism to control the rocking behavior.

3. Test arrangement

3.1 *Washer spring tests*

Before discussing the SCR piers in detail, the cyclic behavior of individual SMA washer springs was examined first. The SMA washer springs used for this study were ordered from SAES Smart Materials Corporation (www.memry.com). The governing geometric parameters, i.e., external diameter (D_e), internal diameter (D_i), height (l_0), thickness (t), and cone angle (θ), are shown in Fig.

1(a). Each single washer spring can provide a compressive deformation of up to 3 mm. Per information from the supplier, the chemical composition of the SMA material was wt.55.87% nickel and wt.44.13% titanium. The austenite finish temperature A_f was lower than 5 °C, indicating that the SMA washer springs exhibit superelasticity at room temperature (the room temperature during the tests was around 18~22 °C).

Fig. 1(a) shows the universal test machine (UTM) and the bespoke testing device used for obtaining the washer spring response. The testing device consisted of a loading bar and a base which were fixed to the top and bottom wedge hydraulic grips, respectively. The load was applied via the loading bar which inserted into the hollowed area of the base. Two testing cases were considered, namely, 1) a single SMA washer spring and 2) a set of four SMA washer springs (two in parallel × two in series). The tests were conducted quasi-statically under displacement control. For the single washer spring test, the specimen was loaded with incremental compressive displacements from 0.5 mm to 2.5 mm with an interval of 0.5 mm, and two cycles were applied per amplitude. For the washer spring set test, the displacement at each amplitude was doubled because of the doubled deformability resulting from the considered stack combination.

Fig. 1(b) shows the typical test results of the SMA washer springs. The single washer spring specimen shows flag-shaped hysteresis with negligible residual deformation and moderate energy dissipation capacity. The hysteresis loops are quite stable, confirming that the component is suitable for repeated use with no need for replacement. “Yielding” of the single washer spring occurs at approximately 8.5 kN, which is followed by a forward transformation plateau with a certain hardening slope. Upon unloading, a reverse transformation plateau is induced which enables deformation recovery. The shape of the hysteretic response of the SMA washer spring set is similar to that of the single washer spring, but both the load resistance and deformation are doubled. This reaffirms the flexibilities of load and deformation provided by the washer springs with different combinations.

3.2 *SCR pier specimen*

A proof-of-concept SCR bridge pier was designed for the experimental program. The geometric configuration and the reinforcement details are shown in Fig. 4. The entire pier was finished by monotonic casting of three parts, i.e., loading head, main pier, and extended pier base, using C30 concrete. A heavy concrete foundation block was additionally produced which was firmly fixed to the strong floor. A groove (slot) was reserved in the foundation block to accommodate the pier base and to guide the rocking response. Two 8 mm-thick steel plate stoppers were installed next to the pier base to prevent large slippage before gap opening. A total of 12 Grade HRB400 (measured f_y = 400.4 MPa) longitudinal rebars with a diameter of 16 mm were uniformly arranged along the circumference of the pier. The corresponding longitudinal reinforcement ratio was 3.4%. Transverse reinforcement (with diameter of 10 mm) was placed with a space of 75 mm. The clear thickness of the cover concrete is 20 mm. A number of PVC tubes were placed at predetermined locations during the pouring of the concrete. After hardening of the concrete, the openings were used to accommodate the constraining anchor bars as well as a central PT tendon which was used to mimic the gravity load applied to the pier. The overall height of the pier, including the loading head and pier base, was 1825 mm. The average compressive strength of 150×150×150 mm cubic concrete blocks measured at the day of testing was 39 MPa.

The pier specimen has four constraining anchor bars, and each anchor bar was equipped with eight SMA washer springs (four pairs stacked in series and each pair consists of two washers stacked in parallel, i.e., 2P×4S). As mentioned, each undeformed individual washer spring can provide a compressive deformation of 3 mm, among which around 0.3 mm has been consumed during the washer spring preloading process. Therefore, the total deformability of a washer spring set was 4 × 2.7 mm = 10.8 mm, corresponding to an available gap opening angle of approximately 1.7% (0.017 radians) for the pier. A total of five tests were conducted successively on the same pier specimen. This is acceptable as the main body of the pier was designed to remain elastic under the considered drift level. The SMA washer springs, which exhibited stable hysteresis under repeated load, were also used repeatedly. The main varying parameters for the different tests were discussed in more detail in

Section 3.3. A consistent preload of 5 kN, calibrated by a torque wrench, was applied to each SMA washer spring set. This preload, together with the "gravity load" applied by the central gravity PT tendon, contribute to the lateral load resistance of the pier prior to gap opening. It is worth mentioning that although some basic design rules are followed (e.g., the pier is designed to stay elastic prior to the locked stage), the selection of the SMA washer configurations was mainly for concept verification purposes and does not necessarily lead to an "optimal" performance of the pier.

3.3 *Test setup and instrumentation*

The test setup for the pier specimen is schematically shown in Fig. 5. The pier was placed vertically on the grooved foundation block, and the four anchor bars passed through the pier base via the reserved openings. The lateral load was applied to the loading head by a double-action electro-hydraulic servo actuator, and the lever arm, i.e., the distance from the centroid of the loading head to the rocking interface, was 1625 mm. The gravity load was simulated by prestressing the central gravity PT tendon to a desirable force level monitored by a load cell.

The arrangement of linear variable differential transformers (LVDTs) for displacement measurement is illustrated in Fig. 5. LVDT #1 was used to obtain the horizontal displacement at the loading point, noting that the drift angle of the pier was calculated by dividing this reading by the lever arm. Two additional pairs of vertical LVDTs (#2 to #5) were adopted to measure the typical compression of the SMA washer spring sets. For each pair, one LVDT was placed at the top shim plate of the washer spring set and the other one was placed on the adjacent concrete surface just below the washer springs. Some additional horizontal LVDTs (#6 to #8) were used to measure the displacement at the other locations of the pier. Six strain gauges were mounted on the longitudinal reinforcement at critical locations where a large bending moment/stress was expected, as shown in Fig. 5.

3.4 *Loading cases and protocols*

To examine the influence of the SMA washer springs on the cyclic behavior of the pier specimen under different axial load levels, a total of five loading cases (tests) were carried out. As

shown in Table 1, three levels of initial axial (gravity) load, i.e., G = 0 kN, G = 75 kN and G = 140 kN, were considered. The latter two correspond to nominal axial load ratios (G/Af_c) of 3.5% and 6.7%, respectively, where A = cross-section area of pier, and f_c = nominal compressive strength of concrete. One limitation of using the PT tendon to mimic the gravity load is that the axial load would keep increasing as the gap opening of the rocking interface developed. A more reasonable consideration of the gravity load can be realized via numerical studies, as discussed later in Section 4. Under each axial load level, two tests, one with SMA washer springs and the other one without the springs, were carried out. The central gravity PT tendon was then removed, and an additional (the fifth) test was conducted on the pier specimen in the absence of the axial load. For ease of identification, each loading case was assigned with a test code, as given in Table 1.

The lateral load was applied quasi-statically with displacement control. Given the limited deformability of the considered SMA washer spring sets, the maximum lateral displacement at the centroid of the loading head was taken as 27.5 mm (i.e., 1625 mm × 1.7%) for the first four tests, such that the main body of the pier remained elastic and hence had a good condition for repeated use. For the final test, the maximum lateral displacement was slightly extended until the SMA washer springs were fully "flattened", and in addition, a clear increase in the load resistance, indicating the occurrence of the "locked" stage, was observed. The lateral displacement was increased incrementally with a uniform interval until reaching the maximum predefined drift angle, and for each amplitude, three repeated cycles were applied. A shortcoming of the present work is that the final collapse mode of the pier was not fully revealed. An obvious damage to the RC pier is expected if the specimen is further loaded with larger amplitudes.

4. Test results and discussions

4.1 *Overview of test phenomena*

The test specimen showed anticipated gap-opening deformation mode, as typically shown in Fig. 6. Apart from very small cracks found on the surface of the pier immediately above the pier base, as well as minor spalling of the pier base near the turning point, no other visual damage was observed

during the entire testing process. The small cracks on the pier surface were fully closed and visually undetectable when the pier returned to the upright position. At the maximum considered lateral displacement, obvious gap opening was observed at the rocking interface, and the SMA washer springs further away from the turning point were visually flattened. These observations are consistent with the design intention that the inelastic deformation demand of the pier system is largely provided by the SMA washer springs, while the remaining parts are generally damage free.

4.2 *Hysteretic curves*

The lateral load-drift angle hysteretic curves obtained from the five tests are shown in Fig. 7. The key mechanical properties, including the initial/post-yield stiffness, yield strength, and energy dissipation characteristics, are summarized in Table 1. The initial linear stage of the hysteretic curves is related to the elastic deformation of the pier plus other possible sources of displacement such as slippage and softening of the turning point prior to gap opening. After decompression, the pier started to rock and the hysteretic curve advances into the inelastic stage. For the cases where no SMA washer spring was employed, an elastic bilinear response with no energy dissipation is exhibited. It should be noted that the drop of the inelastic plateau in test G75 was due to the unexpected slippage of the PT tendon anchorage, and this issue was addressed for the subsequent tests. The presence of the washer springs clearly increases the lateral load resistance and makes certain contribution to energy dissipation, but the initial stiffness is not remarkably influenced. This is not surprising, as the stiffness response of the pier before decompression is not directly relevant to the behavior of the SMA washer springs. On the other hand, the post-yield stiffness is indeed increased due to the use of the SMA washer springs. For test G0W, the lateral load starts to increase quickly when the drift angle exceeds 1.7%, which is due to the fully consumed deformability of the SMA washer spring sets. When the washer springs are fully flattened, further drift angle demand has to be provided by the flexural deformation of the pier, which echoes the design principle discussed in Section 2.

Importantly, the pier specimen exhibits very stable hysteretic curves under the successive loading cases, and no evident deterioration in the strength and stiffness responses is observed. In

addition, no residual deformation is seen when the lateral load is removed. These clearly indicate that the proposed pier system is fully recoverable when subjected to multiple earthquake excitations (e.g., main-shock and after-shock sequences) with no need to repair. From an energy dissipation point of view, the energy dissipation per cycle (W_D) and equivalent viscous damping (EVD) are given in Table 1. The EVD is a dimensionless energy dissipation index as expressed by:

$$EVD = \frac{W_D}{4\pi W_E} \tag{7}$$

where W_E is the energy absorbed by a corresponding linear elastic system. The pier specimen shows modest energy dissipation capacity which is offered by the SMA washer springs. An increase in the axial load leads to a decreased EVD. The relatively small EVD observed in the pier specimen is mainly attributed to the small-size SMA washer springs used in this proof-of-concept study. Some other influential factors are later explained in the numerical study.

4.3 *Supplemental test data*

The deformation of the specimen can be further revealed by the LVDT and strain gauge readings. The local compressive deformation of the SMA washer spring set is shown in Fig. 8(a). As expected, the washer springs further away from the rotation center were significantly compressed at large drift angles. It is also confirmed that the compressive deformation was induced in the washer springs only after the occurrence of decompression (gap opening). Increasing the axial load postpones the inception of gap opening, which is in line with the trend revealed by the lateral load-drift angle curves. As a result, at the same drift angle level, the compressive deformation of the washer springs is reduced when the axial load is increased. There seems to be an upper limit of the washer spring deformation (close to 10 mm) for test G0W, a phenomenon which echoes the locked stage as indicated by the sudden increase in the load resistance in the lateral load-drift angle curve.

The measured lateral displacements at the mid-height of the pier base (LVDT #7) are shown in Fig. 8(b). A small movement of the pier base is observed at small drift angles prior to decompression, which is due to the minor initial slippage between the pair base and the foundation

block. Further slippage was prevented once the pier started to rock or when the pier touched against the steel plate stopper. The maximum LVDT reading at the mid-height of the pier base is around 2.5 mm, which is mainly caused by the inclination of the pier during the rocking process. Figs. 8(c) and 8(d) show the typical strain gauge readings at the critical locations of the longitudinal reinforcement. The maximum measured microstrain is approximately ε_{μ} = 2200 (for test G140W) which is slightly larger than $\varepsilon_{y} \approx$ 2000, suggesting that the reinforcement experienced minor yielding under the maximum considered drift angle. For the remaining four tests, the measured microstrain is always less than 2000 and therefore the reinforcement stayed elastic. Increasing the initial axial load tends to increase the reinforcement strain, which is caused by the larger lateral load sustained by the pier and hence larger bending moment induced at the bottom of the pier. The strain gauge reading highlights the importance of ensuring sufficient reinforcement ratio for the proposed pier type, because unwanted early flexural yielding would occur at the bottom of the pier if the longitudinal reinforcement ratio is insufficient.

5. Numerical study

Following the experimental study, a numerical investigation was conducted with the following purposes: 1) to enable a parametric study which further reveals the influences of extended design parameters on the pier behavior; and 2) to propose amended SCR piers which potentially have improved hysteretic performance.

5.1 *Modelling strategy and validation*

Commercial finite element (FE) program ABAQUS [54] was employed to simulate the SCR piers. An overview of the pier model and the meshing scheme are shown in Fig. 9(a). C3D8R solid elements (i.e., 8-node linear brick elements with reduced integration and hourglass control) were used to model the main components, including the pier, foundation block, strong constraining anchor bars, shim plates and nuts. The reinforcement was modelled using truss elements T3D2 which were embedded within the concrete. S4R elements (4-node shell elements with isoparametric reduced-integration) were used to model the SMA washer spring sets. The contact between the washer springs

stacked in parallel was considered by defining a hard contact behavior. For the contact between the washer springs stacked in series, a "coupling" command was used such that the springs could move in a synchronous way. A hard contact was also defined between the pier base and the foundation block, and the friction coefficient was assumed to be 0.4 [55]. The boundary conditions and the loading sequences of the model were consistent with the test arrangement. The preload was first applied to the SMA washer springs via the "bolt load" command, and then the prestress of the gravity PT tendon was exerted using a temperature-decreasing method. The lateral load was finally applied according to the predefined loading protocols. The entire analysis was conducted with the static solver.

For SMA material modelling, a built-in Auricchio's model was employed which is capable of capturing the fundamental superelastic behavior of the washer springs [56]. The key input parameters for the SMA material are summarized in Table 2 and are explained in Fig. 1(a). The SMA material properties were determined according to the typical values reported in the literature [38, 43]. For the steel components, a bilinear kinematic hardening material model with the von Mises yield criterion was adopted. A concrete damaged plasticity (CDP) model was employed to consider the nonlinear behavior of concrete subjected to cyclic loading. The stress-strain relationship in compression follows linear ascending stage, nonlinear ascending stage and post-limit descending stage successively. The model also describes an initial linear ascending response in tension, followed by a descending branch after attaining the crack strength. The unloading responses in compression and tension are controlled by damage variables d_c and d_t, respectively, which are related to the corresponding inelastic strain. More details of the CDP model can be found in the ABAQUS user's manual [54] as well as other literatures [57].

The behavior of individual SMA washer spring models is first compared with the test results, as shown in Fig. 1(b). Good agreements are observed, although the load resistance at large deformation is slightly underestimated, which is probably due to an inadequate consideration of the complex interaction between these washer springs. Fig. 9(b) shows the typical deformation mode of the pier model, where the gap opening response is clearly observed, and the "squeezing" of the SMA

washer springs is well captured. The predicted hysteretic response also agrees reasonably well with the test result. The discrepancy may be due to the following reasons: 1) the complex nonlinear behavior of the concrete pier base at the turning point is not accurately predicted by the present model, 2) the pier specimen was used repeatedly in the test program, and the resulting damage accumulation is not considered in the current numerical model, and 3) other sources of displacement such as initial slippage are not taken into account. Regardless of the simplifications considered in the numerical model, the essential rocking behavior of the pier at the various stages is adequately captured, and the local deformation of the SMA washer springs agrees very well with the test observation.

5.2 *Considered parameters*

A more comprehensive parametric study is carried out following the validation study. The considered parameters are summarized in Table 3. Three different axial load ratios ranging from 3.5% to 14% are considered, which are believed to cover typical gravity load levels for bridge piers in practice. It should be noted that a constant vertical load is applied to the pier in the parametric study models, in contrast to the use of the PT tendons for simulating the gravity load in the tests. Moreover, three different preloads (zero preload, 5 kN, and 10 kN) are considered for each SMA washer spring set. Another important parameter is the stack pattern (combination) of the SMA washer springs. In this study, three stack patterns are considered, namely, 2P×4S (reference case), 1P×8S, and 4P×2S. Compared with the reference case, 1P×8S leads to halved load resistance but doubled deformability, and 4P×2S leads to doubled load resistance but halved deformability. The total number of the washer springs for the three cases is unchanged. Finally, given the relatively small EVD observed for the SCR piers, especially under large axial load ratios, extra metallic damping components are installed at the gap opening interface. For ease of installation and replacement, the feasibility of adopting steel angles as an extra source of energy dissipation is preliminarily examined in this study. It should be noted that many other damping devices (e.g., friction damper, BRB-typed device, U-shaped damper, viscous damper, etc.) can be used to serve a similar purpose.

5.3 *Parametric study results*

Fig. 10 compares the hysteretic responses of the SCR piers designed with the different parameters. The axial load ratio is shown to have a significant influence on the "yield" resistance of the pier, as shown in Fig. 10(a). In fact, the observed yield resistance corresponds to the decompression resistance of the pier. In other words, the larger the axial load is, the larger the lateral load is required to initiate gap opening. The initial stiffness, which is mainly determined by the flexibility of the pier itself before decompression, is not evidently affected by the axial load. As the total energy dissipation per cycle is mainly contributed by the SMA washer springs, an upward movement of the hysteretic loops, with no significant change in the total hysteretic loop area, is observed with an increase in the axial load. This change also leads to a deceased EVD (which can be seen from Eq. (7)). Another important finding is that under the load ratio of 14%, degradation of the hysteretic response is observed with increasing drift angles, which is caused by severe pier damage. It is also deduced, although not directly shown in the current model, that significant crushing would occur at the turning point under a large axial load ratio. Therefore, the efficiency and attraction of the proposed SCR piers may be compromised because of these undesirable phenomena. It is suggested in practical design that an upper limit of axial load ratio is defined for the SCR piers. Based on the limited experimental and numerical data obtained from this study, 10% seems to be an appropriate axial load ratio limit, although further experimental evidence is needed in order to draw a more solid conclusion.

Compared with the axial load ratio, the preload applied to the SMA washer spring sets has a less critical influence on the pier response, probably because of the small-size SMA washer springs used in the reference model. As shown in Fig. 10(b), the yield resistance (when gap opening just happens) slightly increases with an increase in the preload, but the initial stiffness is not influenced, which has been explained previously. It is also observed that the locked stage is postponed when a smaller preload is applied. On the other hand, the hysteretic behavior of the pier is remarkably changed by using the different stack patterns of the SMA washer springs, as shown in Fig. 10(c). Although the yield resistance is not affected by the stack pattern because of the same axial load ratio

and washer spring preload considered for the three models, the post-yield stiffness increases significantly when more SMA washer springs are stacked in parallel (e.g., 4P×2S), and this is accompanied by a remarkable increase in the energy dissipation per cycle. For the case of 1P×8S, the energy dissipation capability is decreased to almost negligible levels because the inelastic deformation of each individual washer spring is not sufficiently mobilized at the considered drift angles. As increasing load resistance and deformability are contradictory objectives provided that the total number of washer springs are not changed, the locked stage occurs much earlier for the case of 4P×2S due to the decreased total deformability of each washer spring set. Once the pier is locked, damage first occurs at the bottom of the RC pier (plastic hinge region) and then propagates upwards with an increase in the drift ratio. Residual deformation is also induced due to the permeant flexural deformation of the RC pier. In practice, whether to allow such damage depends on the design intention.

Finally, the effectiveness of adding extra sources of energy dissipation is shown in Fig. 10(d). By simply installing two small Q235 steel angles (dimensions are given in Fig. 4) at the gap opening interface, the hysteretic loop is significantly widened, and the energy dissipation per cycle is increased by approximately 150%. However, the increase in energy dissipation is realized at the cost of reduced self-centering capability, where a static residual drift angle of 0.2% is induced after the final cycle. The results warn that a balance needs to be maintained between energy dissipation and self-centering capability. If no static residual deformation is permitted, the main design principle is to ensure that the available restoring moment is no less than the reverse moment caused by the steel angles. Considering the fact that the "actual" residual deformation under dynamic shakedown is often smaller than the static residual deformation, i.e., a well-known phenomenon called "probabilistic self-centering", the "no static residual deformation" rule may be relaxed. More specific design recommendations can be made by system-level dynamic analysis which is, however, beyond the scope of this study.

6. Summary and conclusions

A new type of SCR bridge piers equipped with novel SMA washer springs has been discussed in this study. The proposed system aims to mitigate the damage to the main body of the pier and to eliminate residual deformation after earthquakes. The system can be considered as an alternative solution to the existing PT-based rocking piers, but potentially with some extra benefits. The study commenced with five tests on a proof-of-concept SCR pier specimen with varying axial load ratios and SMA washer spring arrangements. This was followed by a numerical study concerning an extended range of parameters. The concept of the proposed SCR bridge pier has proved an initial success. According to the experimental and numerical studies, the main comments and conclusions are summarized as follows.

- SMA washer springs are capable of providing stable flag-shaped hysteresis with negligible residual deformation and moderate energy dissipation capacity. They could be used repeatedly with no need for replacement, highlighting the great potential of such components for seismic resilient systems.
- The proposed SCR pier has a quite straightforward load resisting mechanism. The pier specimen showed anticipated gap-opening deformation mode under an increasing lateral load, a behavior which effectively mitigate the damage to the pier. Minor crushing of the concrete was observed at the turning point, and such behavior is practically unavoidable for any rocking piers unless a special treatment on the rocking interface is employed (e.g., rounding the edge or adding protective steel shim plates).
- The initial stiffness of the SCR pier prior to decompression is mainly governed by the flexural flexibility of the pier itself. The actual stiffness could also be related to other possible sources of displacement/deformation such as slippage and softening of the turning point. The yield resistance upon decompression is largely determined by the applied gravity load as well as the preload applied to the SMA washer springs.
- The available rocking rotation of the SCR pier after decompression but before the locked stage depends heavily on the deformability of the SMA washer spring sets. Once the washer springs

are fully compressed, the pier advances into the locked stage and then behaves similarly to conventional fixed base piers. In the present study, a flexible rocking rotation of up to 2% drift angle is considered, but no further effort is made towards the optimal design of such flexible rotation. This is reserved for future system level analysis.

- The post-yield inelastic responses of the pier could be readily tuned by considering various stack combinations of the SMA washer springs. In particular, increased post-yield stiffness and energy dissipation are enabled by introducing more washer springs stacked in parallel, and on the other hand, an increase in the available flexible rocking rotation prior to the locked stage could be achieved by introducing more washer springs stacked in series.
- The energy dissipation of the proposed pier is mainly offered by the SMA washer springs and the resulting EVD is typically less than 10%, depending on the axial load and the arrangement of the SMA washer springs. Adding steel angles at the gap opening interface is found to be an effective yet simple solution, and it is believed that many other approaches could work the same way.

7. Acknowledgements

The financial support from the Natural Science Foundation of China (NSFC) with Grant Nos. 51978513 and 51778456 is gratefully acknowledged. Support for this study was also provided by the Shock and Vibration of Engineering Materials and Structures Key Laboratory of Sichuan Province.

8. References

[1] Kawashima K, MacRae GA, Hoshikuma J, Nagaya K. Residual displacement response spectrum. Journal of Structural Engineering 1998; 124(5):523–530.

[2] Jiang ZQ, Lan T, Dou C, Wu Y, Zhang H. Cyclic loading tests of earthquake-resilient prefabricated cross joint with single FCP. Journal of Constructional Steel Research 2020; 164, 105752.

[3] Jiang ZQ, Yang XF, Dou C, Zhang A, Li C. Cyclic testing of replaceable damper: Earthquake-resilient prefabricated column-flange beam-column joint. Engineering Structure 2019; 183, 922-936.

[4] Mander J B, Cheng CT. Seismic resistance of bridge piers based on damage avoidance design.Technical Rep. NCEER-97-0014, NCEER, Dept. of Civil and Environmental Engineering, State Univ. of New York at Buffalo, Buffalo, NY, 1997.

[5] Palermo A, Pampanin S, Marriott D. Design, modeling, and experimental response of seismic resistant bridge piers with posttensioned dissipating connections. Journal of Structural Engineering 2007; 133(11):1648–1661.

[6] Solberg K, Mashiko N, Mander JB, Dhakal RP. Performance of a damage-protected highway bridge pier subjected to bidirectional earthquake attack. Journal of Structural Engineering 2009; 135(5):469–478.

[7] Marriott D, Pampanin S, Palermo A. Quasi-static and pseudo-dynamic testing of unbonded post-tensioned rocking bridge piers with external replaceable dissipaters. Earthquake Engineering & Structural Dynamics 2009; 38(3): 331–354.

[8] Marriott D, Pampanin S, Palermo A. Biaxial testing of unbonded post-tensioned rocking bridge piers with external replaceable dissipaters. Earthquake Engineering & Structural Dynamics 2011; 40(15): 1723–1741.

[9] Guerrini G, Restrepo JI, Massari M, Vervelidis A. Seismic behavior of posttensioned self-centering precast concrete dual-shell steel columns. Journal of structural engineering 2015; 141(4): 04014115.

[10] Rahmzadeh A, Alam MS, Tremblay R. Analytical Prediction and Finite-Element Simulation of the Lateral Response of Rocking Steel Bridge Piers with Energy-Dissipating Steel Bars. Journal of Structural Engineering 2018; 144(11): 04018210.

[11] Guo A, Li Z, Li H, Ou J, Experimental and analytical study on pounding reduction of base-isolated highway bridges using MR dampers, Earthquake Engineering and Structural Dynamics 2009; 38:1307–1333.

[12] Varela S, Saiidi M, A bridge column with superelastic NiTi SMA and replaceable rubber hinge for earthquake damage mitigation, Smart Material and Structure 2016; **25** 075012.

[13] Andisheh K, Liu R, Palermo A, Scott A. Cyclic Behavior of Corroded Fuse-Type Dissipaters for Posttensioned Rocking Bridges. Journal of Bridge Engineering 2018; .1943-5592.0001197.

[14] Guo T, Cao Z, Xu Z, Lu, S. Cyclic load tests on self-centering concrete pier with external dissipators and enhanced durability. Journal of Structural Engineering 2016; 142(1): 04015088.

[15] Chou CC, Chang HJ, Hewes JT. Two-plastic-hinge and two dimensional finite element models for post-tensioned precast concrete segmental bridge columns. Engineering Structures 2013; 46: 205–217.

[16] Shim CS, Chung YS, Yoon JY. Cyclic behavior of prefabricated circular composite columns with low steel ratio. Engineering Structures 2011; 33(9): 2525-2534.

[17] Shim CS, Chung CH, Kim HH. Experimental evaluation of seismic performance of precast segmental bridge piers with a circular solid section. Engineering Structures 2008; 30(12): 3782-3792.

[18] Wang JC, Ou YC, Chang KC, Lee G C. Large-scale seismic tests of tall concrete bridge columns with precast segmental construction. Earthquake Engineering & Structural Dynamics 2008; 37(12): 1449–1465.

[19] Hewes JT, Priestley MJN. Seismic design and performance of precast concrete segmental bridge columns. Rep. No. SSRO-2001/25, Dept. of Structural Engineering, Univ. of California at San Diego, La Jolla, CA, 2002.

[20] Motaref S, Saiidi M, Sanders D. Shake table studies of energy-dissipating segmental bridge columns. Journal of Bridge Engineering 2014; 19(2): 186–199.

[21] Sideris P, Aref AJ, Filiatrault A. Large-scale seismic testing of a hybrid sliding-rocking posttensioned segmental bridge system. Journal of Structural Engineering 2014; 140(6): 04014025.

[22] Sideris P, Aref A J, Filiatrault A. Quasi-static cyclic testing of a large-scale hybrid sliding-rocking segmental column with slip-dominant joints. Journal of Bridge Engineering 2014; 19(10): 04014036.

[23] Roh H, Reinhorn AM. Hysteretic behavior of precast segmental bridge piers with superelastic shape memory alloy bars. Engineering Structures 2010; 32(10): 3394-3403.

[24] Elgawady MA, Dawood HM. Analysis of segmental piers consisted of concrete filled frp tubes. Engineering Structures 2012; 38(4): 142-152.

[25] Fang C, Yam MCH, Lam ACC, Xie LK. Cyclic performance of extended end-plate connections equipped with shape memory alloy bolts. Journal of Constructional Steel Research 2014; 94:122-136.

[26] Wang W, Fang C, Liu J. Self-centering beam-to-column connections with combined superelastic SMA bolts and steel angles. Journal of Structural Engineering ASCE 2017; 143(2):04016175.

[27] Fang C, Wang W, He C, Chen YY. Self-centring behaviour of steel and steel-concrete composite connections equipped with NiTi SMA bolts. Engineering Structures 2017; 150: 390-408.

[28] Speicher MS, Desroches R, Leon RT. Experimental results of a NiTi shape memory alloy (SMA)-based recentering beam-column connection. Engineering Structures 2011; 33(9):2448-2457.

[29] Christopoulos C, Filiatrault A, Uang CM, Folz B. Posttensioned energy dissipating connections for moment-resisting steel frames. Journal of Structural Engineering 2002;128(9):1111-1120.

[30] Garlock MM, Ricles JM, Sause R. Influence of design parameters on seismic response of post-tensioned steel MRF systems. Engineering Structures 2008; 30(4):1037-1047.

[31] Li Z, He M, Wang K. Hysteretic performance of self-centering glulam beam-to-column connections. Journal of Structural Engineering 2018; 144(5):04018031.

[32] Yam MCH, Fang C, Lam ACC, Zhang YY. Numerical study and practical design of beam-to-column connections with shape memory alloys. Journal of Constructional Steel Research 2015; 104:177-192.

[33] Wang B, Zhu S, Qiu CX, Jin H. High-performance self-centering steel columns with shape memory alloy bolts: design procedure and experimental evaluation. Engineering Structures 2019; 182, 446-458.

[34] Wang B, Zhu S, Zhao J, Jiang H. Earthquake resilient RC walls using shape memory alloy bars and replaceable energy dissipating devices. Smart Materials and Structures 2019; 28(6): 065021.

[35] Makris N, Aghagholizadeh M. The dynamics of an elastic structure coupled with a rocking wall. Earthquake Engineering & Structural Dynamics 2017; 46(6): 945-962.

[36] Gur S., Xie Y., DesRoches R., Seismic fragility of steel building frames with superelastic shape memeory alloy dampers: Comparison with yielding dampers, Journal of Intelligent Material Systems and Structures 2019, 30, 18-19.

[37] Lagoudas DC. Shape memory alloys: modeling and engineering applications, Springer TX, USA, 2008.

[38] Wang W, Fang C, Liu J. Large size superelastic SMA bars: heat treatment strategy, mechanical property and seismic application. Smart Materials and Structures 2016; 25(7):075001.

[39] Fang C, Yam MCH, Ma HW, Chung KF. Tests on superelastic Ni–Ti SMA bars under cyclic tension and direct-shear: towards practical recentring connections. Materials and Structures 2015; 48(4):1013-30.

[40] Qiu C, Zhu S. Shake table test and numerical study of self-centering steel frame with SMA braces. Earthquake Engineering & Structural Dynamic 2017; 46:117–137.

[41] Qiu C, Li H, Ji K, Hou H, Tian L. Performance-based plastic design approach for multi-story self-centering concentrically braced frames using SMA braces. Engineering Structures 2017;153: 628-638.

[42] Jani JM, Leary M, Subic A, Gibson MA. A review of shape memory alloy research, applications and opportunities. Materials and Design 2014; 56: 1078-1113.

[43] Wang W, Fang C, Yang X, Chen YY, Ricles J, Sause R. Innovative use of a shape memory alloy ring spring system for self-centering connections. Engineering Structures 2017; 153:503–15.

[44] Fang C, Zhou XY, Osofero AI, Shu Z, Corradi M. Superelastic SMA Belleville washers for seismic resisting applications: experimental study and modelling strategy. Smart Materials and Structures 2016; 25: 105013.

[45] Fang C, Zheng Y, Chen J, Yam MC, Wang W. Superelastic NiTi SMA cables: Thermal-mechanical behavior, hysteretic modelling and seismic application. Engineering Structures 2019, 183: 533-549.

[46] Alam MS, Nehdi M, Youssef, Shape Memory Alloy Based Smart RC Bridges: Overview of State-of-The-Art, Smart Structures and Systems 2008, 367-389.

[47] Ozbulut O. E., Hurlebaus S., Optimal design of superelastic friction base isolators for seismic protection of highway bridges against near-fault earthquakes, Earthquake Engineering and Structural Dynamics 2011, 40(3), 273-291.

[48] Mishra SK, Gur S, Chakraborty S, Stochastic response of bridge isolated by Shape-Memory-Alloy-Rubber Bearing subjected to Random Earthquakes, Journal of Bridge Engineering 2015, 04015071.

[49] Sgambitterra E, Maletta C, Furgiuele F. Modeling and simulation of the thermo-mechanical response of NiTi-based Belleville springs. Journal of Intelligent Material Systems and Structures 2014; 27(1): 445-457.

[50] Speicher M, Hodgson D, DesRoches R, Leon RT. Shape Memory Alloy Tension/Compression Device for Seismic Retrofit of Buildings, Journal of Engineering Materials and Performance 2009; 18(5-6): 746-753.

[51] Fang C, Yam MCH, Chan TM, Wang W, Yang X, Lin XM. A study of hybrid self-centring connections equipped with shape memory alloy washers and bolts. Engineering Structure 2018; 164:155–168.

[52] Ou YC, Chiewanichakorn M, Aref AJ, Lee GC. Seismic Performance of Segmental Precast Unbonded Posttensioned Concrete Bridge Columns. Journal of Structural Engineering 2007; 133(11): 1636-1647.

[53] Bu ZY, Ou YC. Simplified Analytical Pushover Method for Precast Segmental Concrete Bridge Columns. Advances in Structural Engineering 2013; 16(5): 805–822

[54] ABAQUS. Analysis User's manual, v6.14, Dassault Systems Simulia Corp., Providence, USA, 2014.

[55] Farny JA, Melander JM, Panarese WC. Concrete masonry handbook for architects, engineers, builders, 6th Edition, Portland Cement Association, 2008.

[56] Auricchio F, Taylor RL, Lubliner J. Shape-memory alloys: macromodelling and numerical simulations of the superelastic behaviour. Computer Methods in Applied Mechanics and Engineering 1997; 146: 281-312.

[57] Sinha BP, Gerstle KH, Tulin LG . Stress-strain relations for concrete under cyclic loading. ACI Structural Journal 1964; 62(2):195-210.

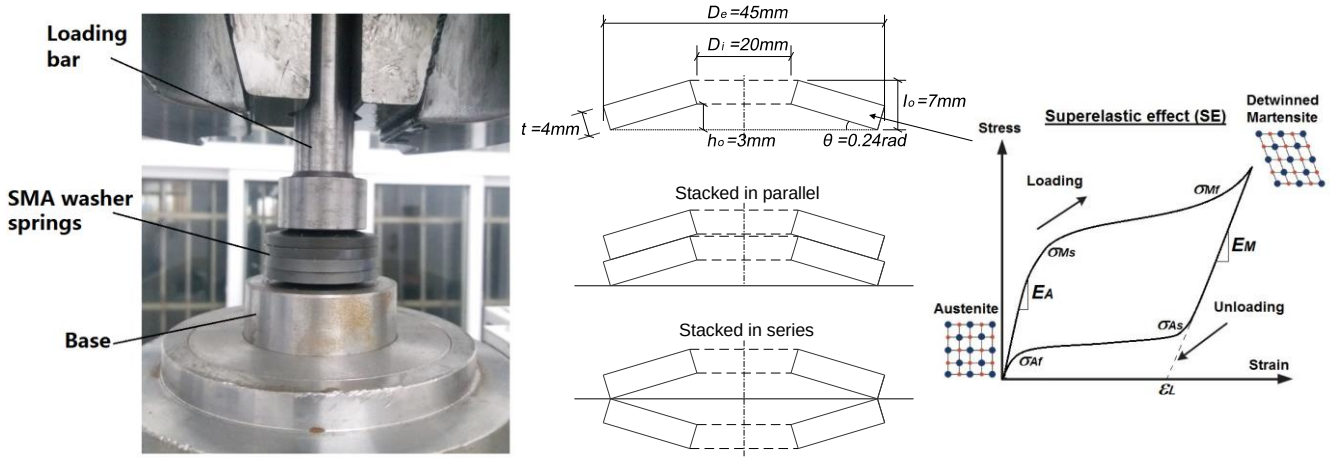

(a)

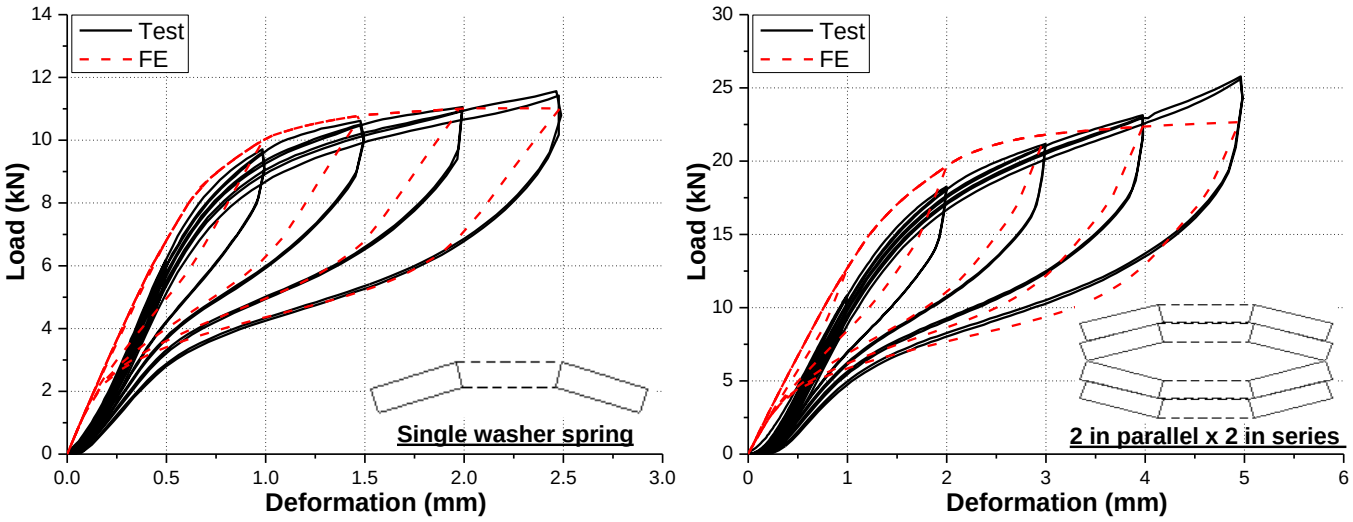

(b)

Fig. 1 SMA washer springs: a) concepts and dimensions, b) cyclic behavior

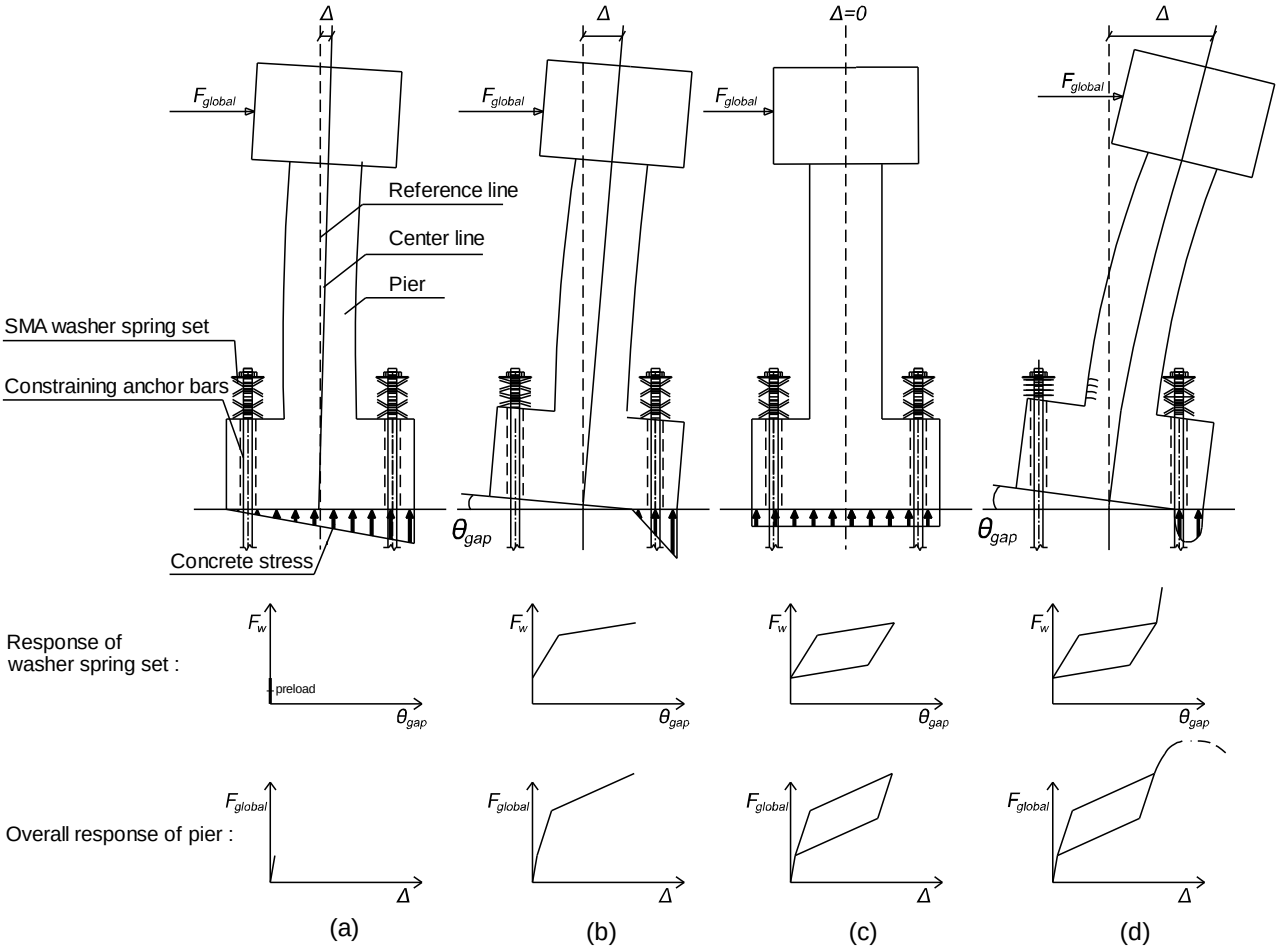

Fig. 2 Working principle of SCR piers with SMA washer springs

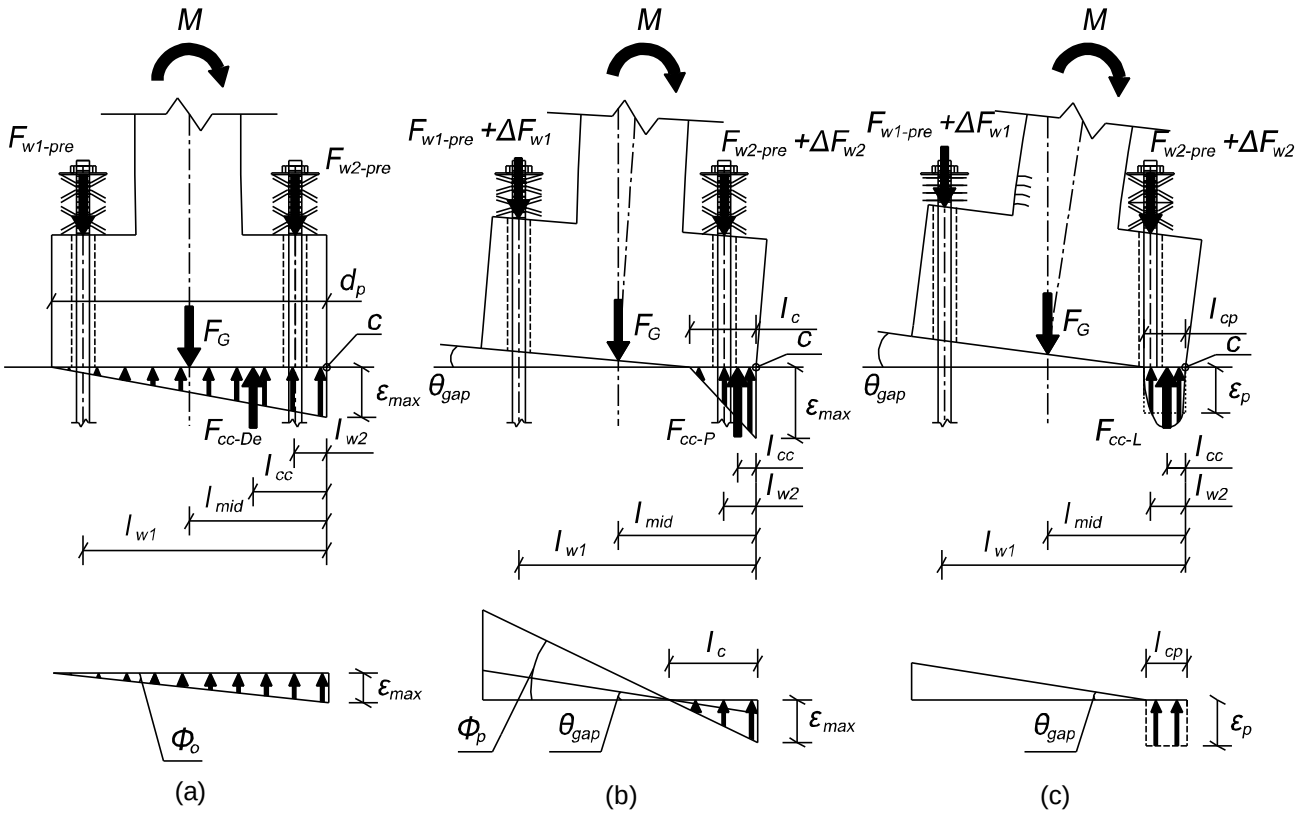

Fig. 3 Force decomposition diagrams: a) decompression stage, (b) post-decompression stage; (c) locked stage

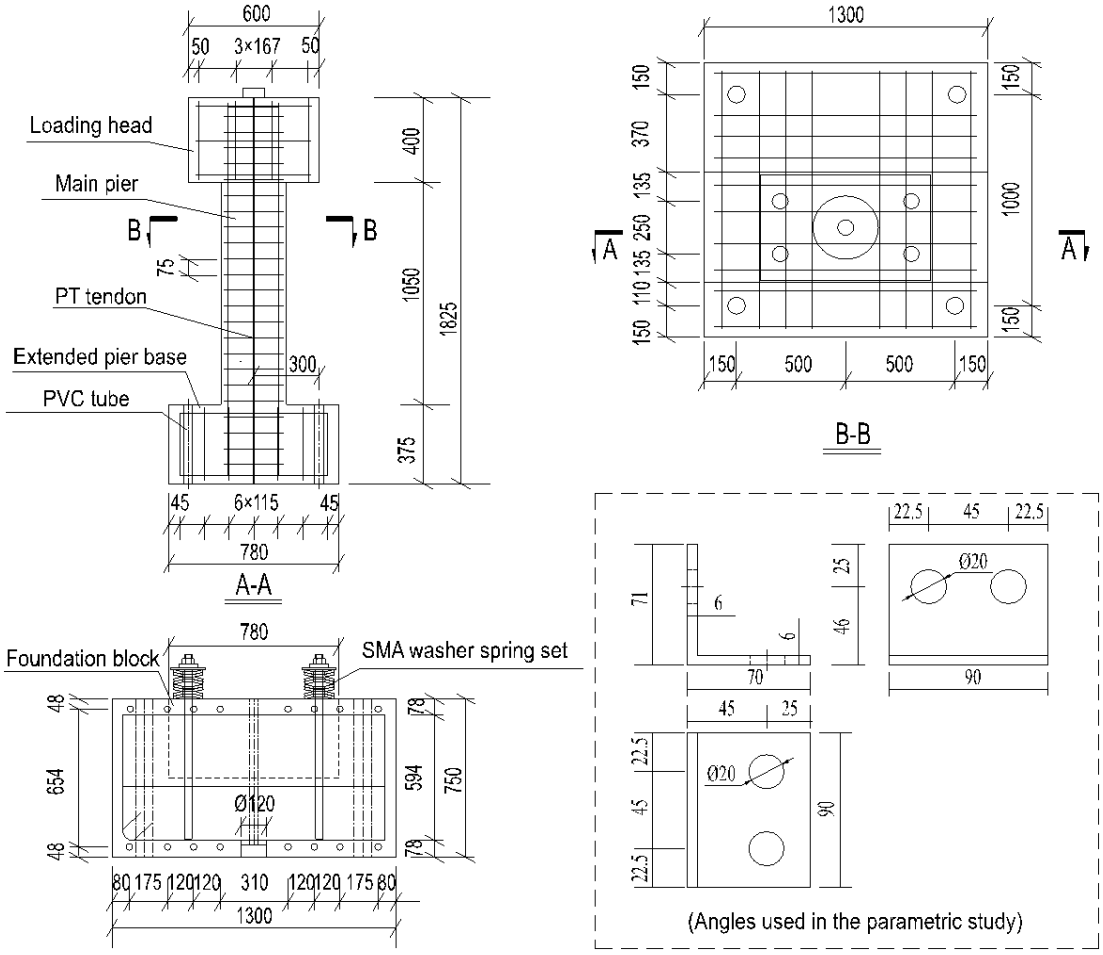

Fig. 4 Design details of pier specimen

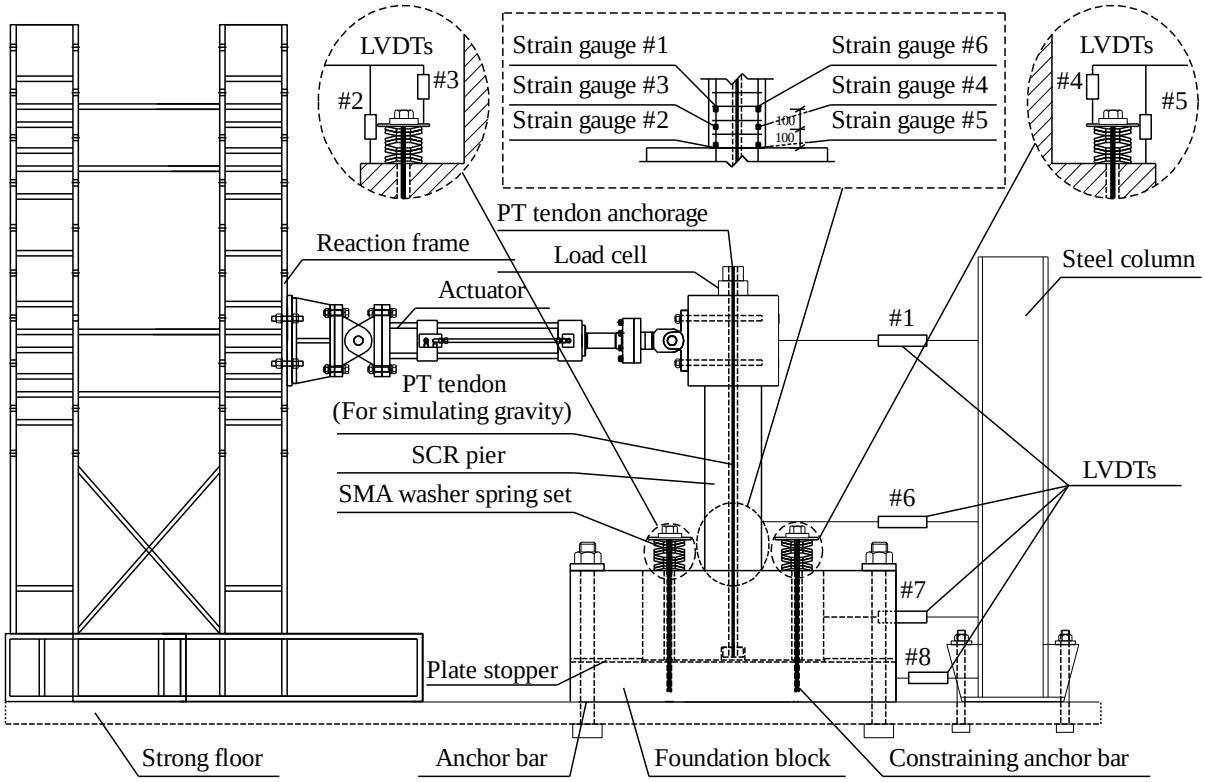

Fig. 5 Test setup and instrumentation

Fig. 6 Observed deformation mode of test specimens

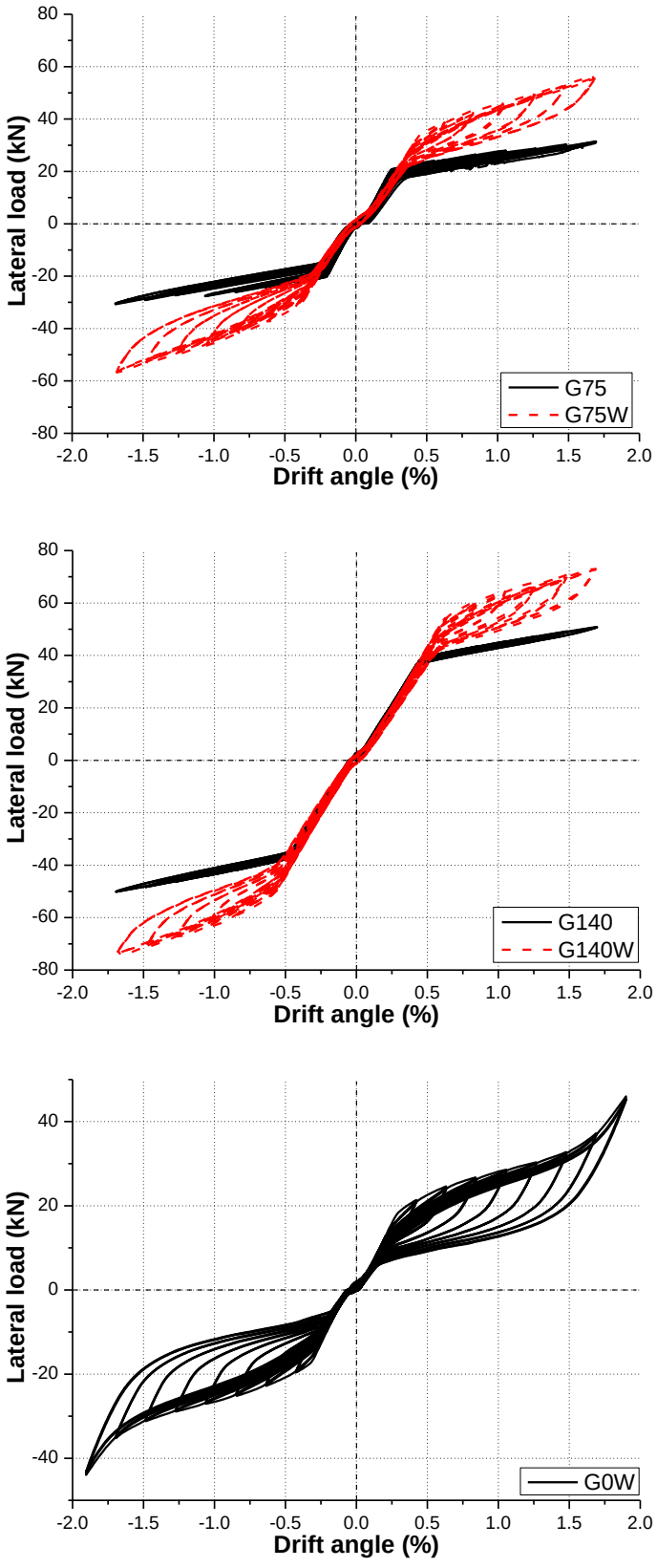

Fig. 7 Lateral load-drift angle hysteretic curves of test specimens

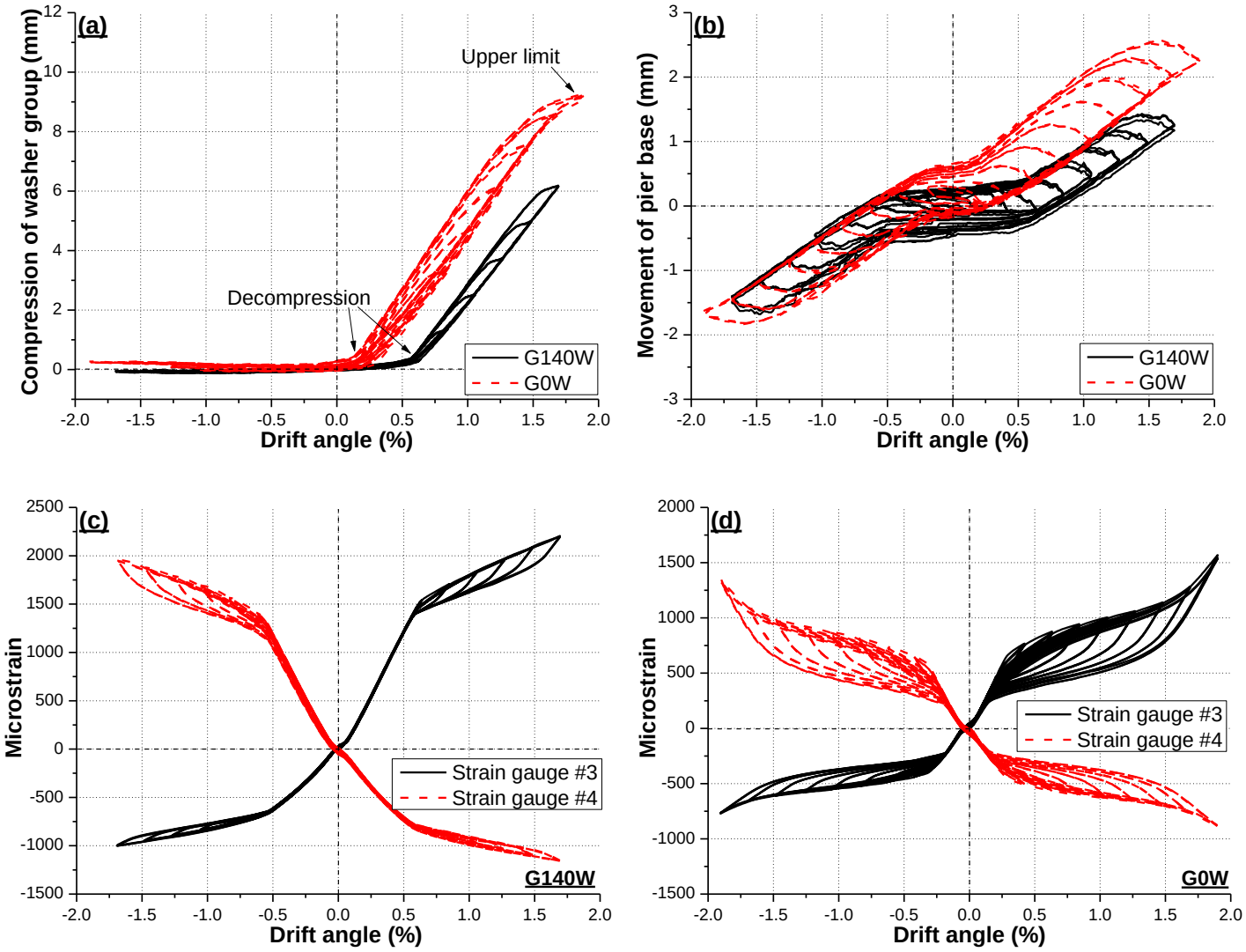

Fig. 8 Supplemental test data from LVDTs and strain gauges

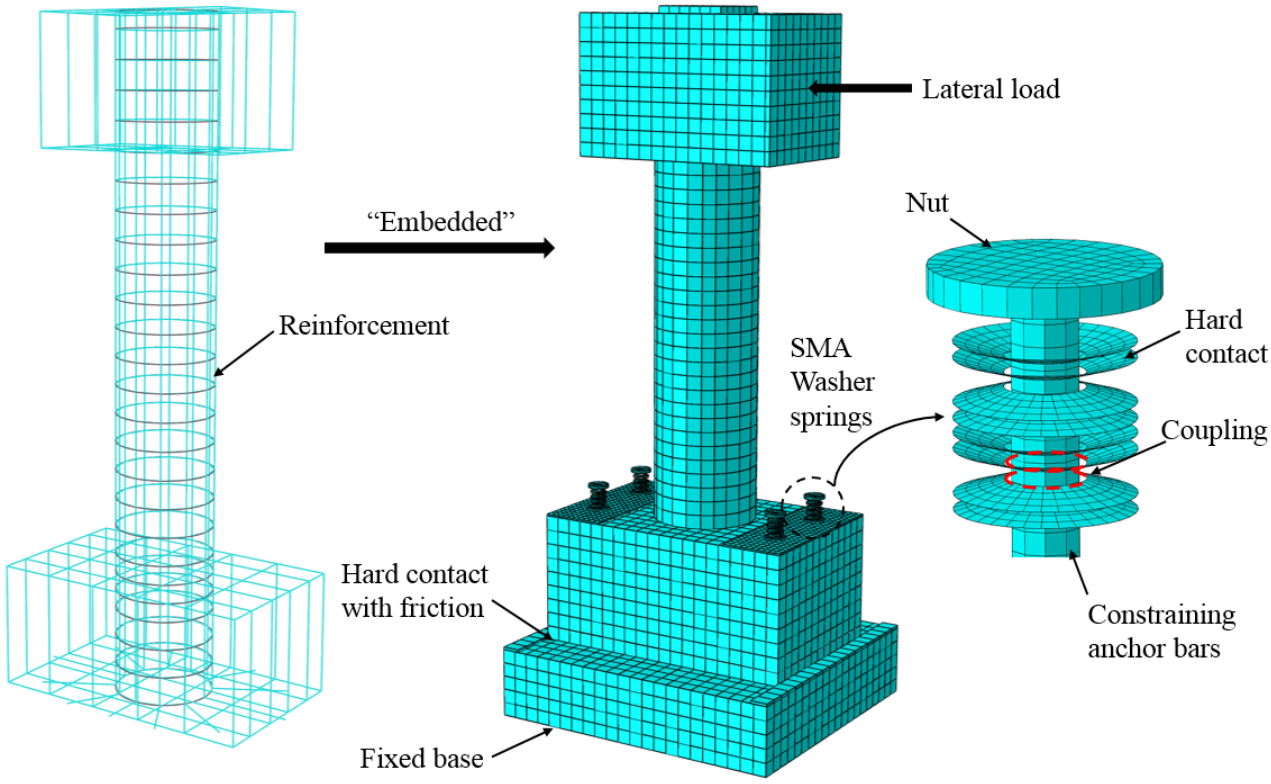

(a)

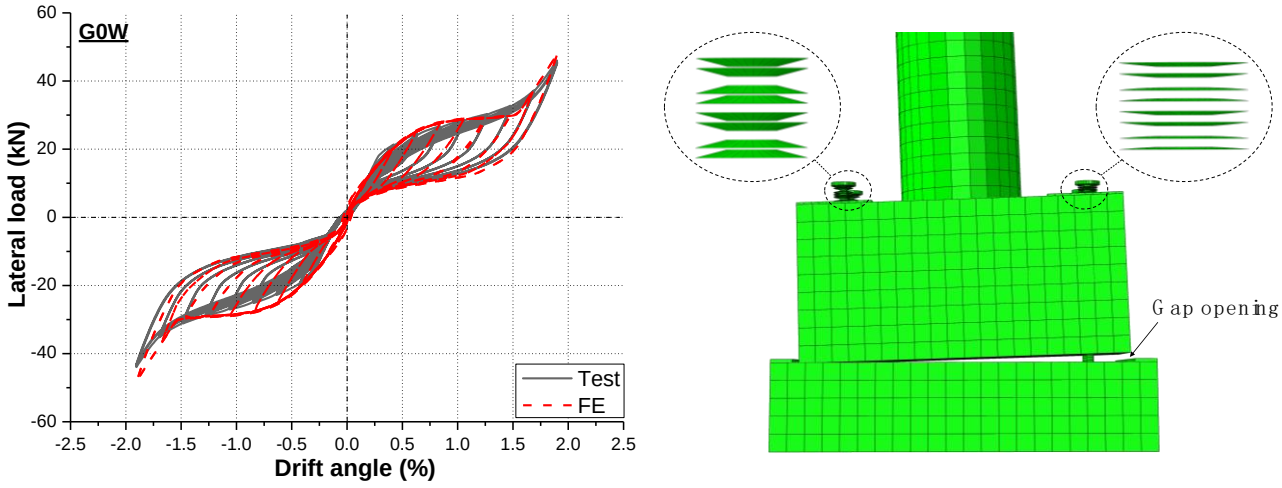

(b)

Fig. 9 Numerical modelling: a) overview of pier model and the meshing scheme, b) predicted pier behavior

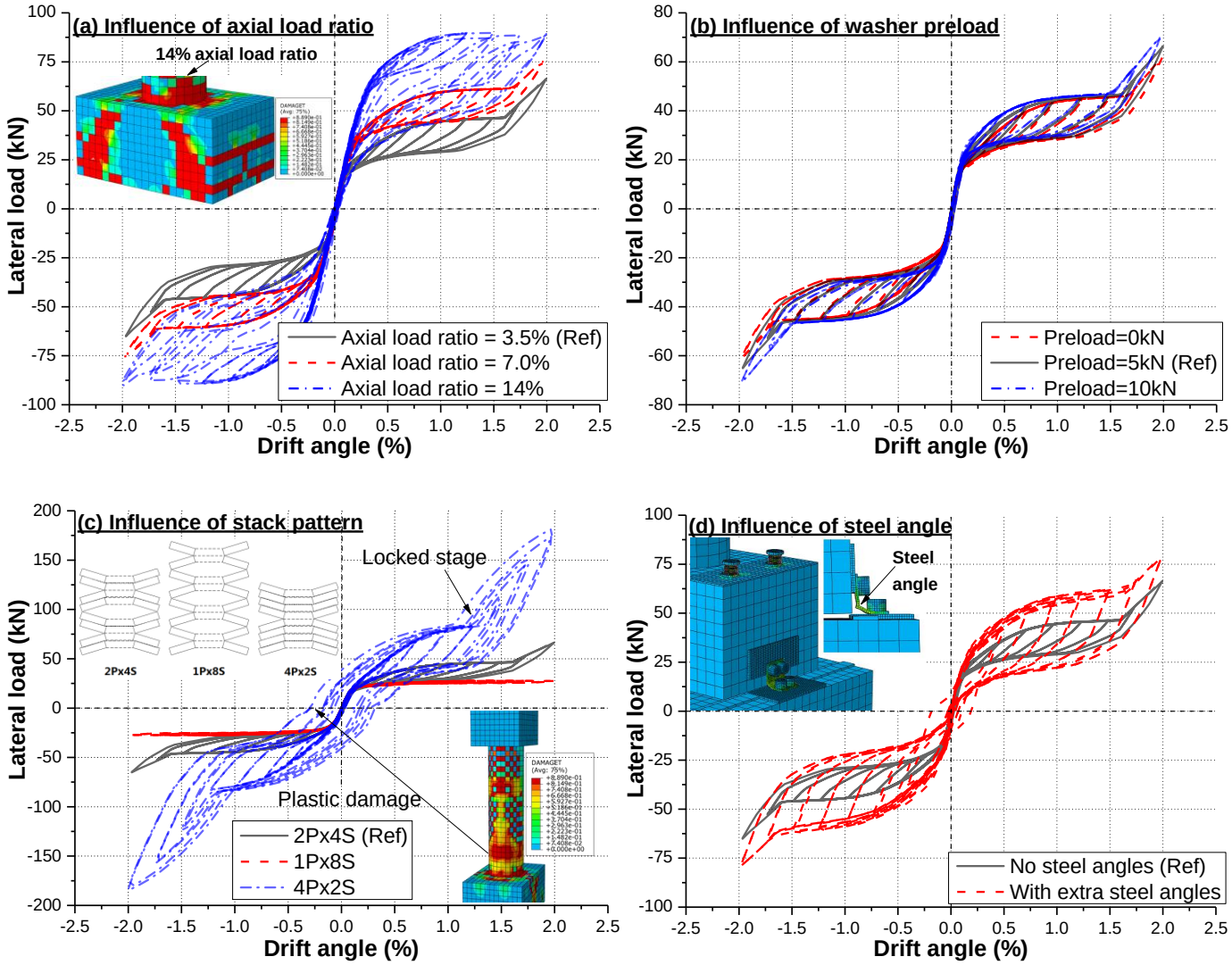

Fig. 10 Parametric study results

Table 1 Loading cases and test results

Test code	Initial gravity load by PT tendon (kN)	With SMA washer springs	"Yield" resistance (kN)	Initial stiffness (kN/mm)	Post-yield stiffness (kN/m)	Energy loss per cycle* (J)	Equivalent viscous damping*
G75	75	No	20.9	6.20	0.56	Negligible	Negligible
G75W	75	Yes	34.1	4.92	1.11	394.3	4.06%
G140	140	No	38.5	5.33	0.59	Negligible	Negligible
G140W	140	Yes	54.8	5.37	1.19	376.4	3.05%
G0W	0	Yes	19.2	4.07	0.60	438.4	7.16%

Note *: typical value based on the behavior at 1.7% drift angle

Table 2 Material properties for simulation of SMA washer springs

Material properties	Values
Forward transformation start stress σ_{Ms}	400 MPa
Forward transformation finish stress σ_{Mf}	600 MPa
Reverse transformation start stress σ_{As}	230 MPa
Reverse transformation finish stress σ_{Af}	75 MPa
Young's Modulus E_A	55 GPa
Young's Modulus E_M	50 GPa
Maximum transformation strain ε_L	5%
Poisson's Ratio v_A	0.33
Poisson's Ratio v_M	0.33

Table 3 Summary of considered parameters

Parameter	Range of parameters
Axial load ratio	**3.5%**, 7%, 14%
Preload of each SMA washer spring group	0, **5kN**, 10kN
Stack pattern of SMA washer spring group	**2P×4S**, 1P×8S, 4P×2S
With extra energy dissipation angles	**No**, Yes

Bold: reference case; "P": in parallel; "S": in series